

Emerging from Water: Underwater Image Color Correction Based on Weakly Supervised Color Transfer

Chongyi Li, *Student Member, IEEE*, Jichang Guo, Chunle Guo

Abstract—Underwater vision suffers from severe effects due to selective attenuation and scattering when light propagates through water. Such degradation not only affects the quality of underwater images but limits the ability of vision tasks. Different from existing methods which either ignore the wavelength dependency of the attenuation or assume a specific spectral profile, we tackle color distortion problem of underwater image from a new view. In this letter, we propose a weakly supervised color transfer method to correct color distortion, which relaxes the need of paired ground truth underwater images for training and allows for the underwater images unknown where were taken. Inspired by Cycle-Consistent Adversarial Networks, we design a multi-term loss function including adversarial loss, cycle consistency loss, and SSIM (Structural Similarity Index Measure) loss, which translates the color of underwater image as if it is taken in the air, and preserves the content and structure of original image. Experiments on underwater images captured under diverse scenes show that our method produces visually pleasing results, even outperforms the art-of-the-state methods. Besides, our method can improve the performance of vision tasks.

I. INTRODUCTION

Recently, ocean engineering and research have increasingly relied on underwater images captured from Autonomous Underwater Vehicles (AUVs) and Remotely Operated Vehicles (ROVs) [1]. However, underwater images usually suffer from degeneration, such as low contrast, color casts, and noise, due to wavelength-dependent light absorption and scattering as well as the effects from low-end optical imaging devices. Such scattering and absorption attenuate the direct transmission and introduce surrounding scattered light. The attenuated direct transmission causes the intensity from the scene to weaker and color casts, while the surrounding scattered light causes the appearance of the scene to be washed out. Besides, the magnitude of attenuation and scattering depend on several complex factors, including water temperature and salinity, and the type and quantity of particulates in the water. Serious degeneration makes it difficult to recover the appearance and color of underwater images. However, color is extremely important for underwater vision tasks and research [2]. Therefore, how to effectively approximate the real color of underwater image has become a significant problem needed to be solved.

This work was supported in part by the National Key Basic Research Program of China (2014CB340403), the National Natural Science Foundation of China (61771334).

Chongyi Li, Jichang Guo and Chunle Guo are with the School of Electrical and Information Engineering, Tianjin University, Tianjin, China (e-mail: lichongyi@tju.edu.cn; jcguo@tju.edu.cn; guochunle@tju.edu.cn).

(Corresponding author: Chunle Guo.)

A number of methods [3]–[16] have been proposed to improve the visual quality of underwater images, ranging from hardware solutions to image dehazing and color correction methods [17], [18]. The hardware solutions [3]–[6] have shown the effectiveness, but these solutions are not applicable to dynamic acquisition. Most of single underwater image restoration methods [7]–[13] are inspired by the outdoor dehazing strategies [19]–[22]. For underwater image color correction, traditional color constancy methods (e.g., Gray World [23], Max RGB [24], White Balance [25], Shades-of-Gray [26], and *et al.*) and their variations are usually employed. Compared with traditional methods based on statistical priors/assumptions obtaining from nature scenes, we bridge the gap between the color of underwater image and that of air image by learning their cross domain relations. We propose an end-to-end model that translating underwater image to air image. In this way, the color casts of underwater images is removed and the performance of vision tasks can be improved since these applications usually assume that the input images are of scene content that are taken in the air. Recently, a semi-supervised learning model for underwater image color correction, named WaterGAN, has been proposed [14]. Unlike this work, our model is no need for a large annotated dataset of images pairs. Besides, WaterGAN shows limitations when it is used to process the underwater images captured under unknown sites. In addition, contrast to translating image style [27], [28], our model learns the semantic color of air image while preserving key attributes such as content and structure.

In this letter, we present a novel weakly supervised solution for underwater image color correction, which is trained to transfer the color of underwater images by mapping them from the scenes of underwater into the scenes of air without any explicit pair labels. Specifically, given an underwater as the input, our model directly outputs an image, where the contents and structure are the same as the input, however, the color of our result is like the color in the air. Though the translated color might not be the “real” color of underwater image, our method can remove the color casts and even improve the performance of vision tasks. In fact, it is impossible that a method recovers the appearance and color of any underwater images when the scenes and light conditions are unknown. Figure 1 shows two examples of our attempts.

Contributions. This letter introduces the following main contributions: (1) Compared to existing priors/assumptions based and semi-supervised methods, to our best knowledge, this is the first attempt to build a weakly supervised model for



Fig. 1. Two examples of our results.

underwater image color correction. Here, “weak supervision” means that our method relaxes the need of paired ground truth underwater images for training and allows for the underwater images unknown where were taken. (2) We tackle underwater image color correction problem from a new angle, which learns a cross domain mapping function between underwater images and air images. (3) A multi-term loss function allows our model capturing context and semantic information, which preserves underwater image content and structure, and just achieves the color of air image.

II. PROPOSED METHOD

Our solution is based upon very recent advances in image-to-image translation networks [29]–[31], which captures special characteristics of one image collection and figures out how these characteristics could be translated into the other image collection, all in the absence of any paired training examples. Our goal is to learn mapping functions between a source domain X (i.e., underwater) and a target domain Y (i.e., air). The inputs are unpaired training image samples $x \in X$ and $y \in Y$. Specifically, our model includes two mappings $G : X \rightarrow Y$ (forward) and $F : Y \rightarrow X$ (backward) given training data $\{x_i\}_{i=1}^N \in X$ and $\{y_i\}_{i=1}^N \in Y$. Following the Cycle GAN [29], we also use two adversarial discriminators D_X and D_Y , where D_X aims to distinguish between images $\{x\}$ and translated images $\{F(y)\}$ when D_Y aims to distinguish between images $\{y\}$ and translated images $\{G(x)\}$. For the generator of forward networks, the loss function includes three terms: adversarial loss for matching the distribution of generated images to the distribution in the target domain, cycle consistency loss to prevent the learned mapping G and F from contradiction each other, and SSIM loss [32] to preserve the content and structure of source images. For the generator of backward networks, the loss function also includes three same terms. The framework of the proposed method is shown in Figure 2. Below, we just present the losses of forward networks and vice versa for backward networks.

A. Adversarial loss

For the mapping function $G : X \rightarrow Y$ and its discriminator D_Y , the adversarial loss can be expressed as:

$$L_{GAN}(G, D_Y, X, Y) = E_{y \sim p_{data}(y)} [\log D_Y(y)] + E_{x \sim p_{data}(x)} [\log(1 - D_Y(G(x)))] \quad (1)$$

where G tries to generate images $G(x)$ that look similar to images from domain Y while D_Y aims to distinguish between translated samples $G(x)$ and real samples y .

B. Cycle consistency loss

We add a cycle consistency loss to constrain the space of possible mapping functions. Cycle consistency means that for each image x from domain X , the image translation cycle should be able to bring x back to the original image, while for each image y from domain Y , the image translation cycle should be able to bring y back to target image. Cycle consistency loss can be expressed as:

$$L_{cyc}(G, F) = E_{x \sim p_{data}(x)} [\|F(G(x)) - x\|_1] + E_{y \sim p_{data}(y)} [\|G(F(y)) - y\|_1]. \quad (2)$$

C. SSIM loss

To preserve content and structure similarity between the original and translated images, SSIM loss [33] is used. First, for pixel p , the SSIM between input image x and translated image $G(x)$ is defined as:

$$SSIM(p) = \frac{2\mu_x\mu_y + C_1}{\mu_x^2 + \mu_y^2 + C_1} \cdot \frac{2\sigma_{xy} + C_2}{\sigma_x^2 + \sigma_y^2 + C_2}, \quad (3)$$

where p is the center pixel of an image patch, x is an image patch $\in X$ with size 13×13 , y is an image patch $\in G(x)$ with size 13×13 , μ_x is the mean of x , σ_x is the standard deviations of x , μ_y is the mean of y , σ_y is the standard deviations of y , σ_{xy} is the covariance of x and y . $C_1=0.02$ and $C_2=0.03$ are default in SSIM loss. In this way, the SSIM value for every pixel between input image x and translated image $G(x)$ is calculated. The SSIM loss can be expressed as:

$$L_{SSIM}(x, G(x)) = 1 - \frac{1}{N} \sum_{p=1}^N (SSIM(p)). \quad (4)$$

where N is the number of pixel in an image.

D. Total loss

Finally, the total loss is the linear combination of the above-mentioned three losses with weights:

$$L_{loss} = \lambda_1 L_{GAN}(G, D_Y, X, Y) + \lambda_2 L_{cyc}(G, F) + \lambda_3 L_{SSIM}(x, G(x)). \quad (5)$$

where weights λ_1 , λ_2 and λ_3 are 1, 1 and 10 based on heuristic experiments on our training data, which makes the order of magnitudes of three components equal because we expect that these three components have equally significant contributions in the final loss function. The optimization of generator G of forward networks is to minimize Equation (5) when the optimization of discriminator D_Y is to maximizing Equation (1). In training process, we alternatively optimize G , D_Y , F , and D_X , respectively.

E. Network architecture and training details

The forward and backward networks have the same architecture. Following Cycle GAN [29], we adapt the architecture [34] for our generators and use 70×70 PatchGANs [35]–[37] as our discriminators. For the limited space, more details can be found in [29]. To train our model, we collect a dataset from Internet, which contains 3800 underwater images and 3800 air images. After that, those images are resized to 256×256 based

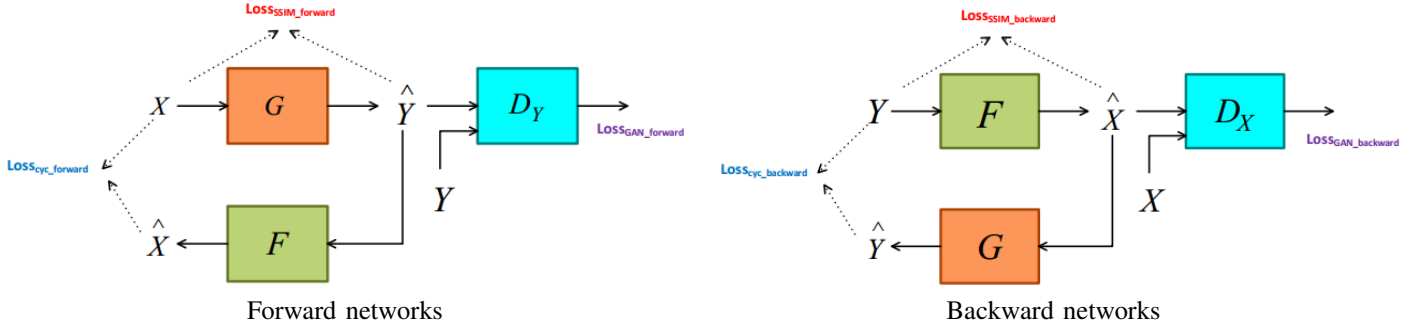


Fig. 2. A diagram of our framework. Our model contains two mapping functions $G : X \rightarrow Y$ (forward) and $F : Y \rightarrow X$ (backward), and associated adversarial discriminators D_Y and D_X .



Fig. 3. Our training samples.

on our limited memory and the architectures of discriminators. Figure 3 shows several training samples.

In addition, to stabilize our model training procedure, we replace the negative log likelihood objective by a least square loss in Equation (1). Equation (1) is rewritten as :

$$L_{GAN}(G, D_Y, X, Y) = E_{y \sim p_{data}(y)}[(D_Y(y) - 1)^2] + E_{x \sim p_{data}(x)}[D_Y(G(x))^2]. \quad (6)$$

Discriminators D_X and D_Y were updated by a history of generated images rather than the ones produced by the latest generative networks. We trained our model using ADAM [38] and set the learning rate to 0.0002 and momentum to 0.5. The batch size was set to 1. We implemented the proposed network with the TensorFlow framework and trained it using NVIDIA TITAN X GPU. It took 15 hours to optimize our model. This code will be made publicly available.

III. EXPERIMENTS

We compare the proposed model with several state-of-the-art methods: image-to-image transfer method (*i.e.*, CycleGAN [29]), color constancy method (*i.e.*, Gray Word (GW) [23]), image enhancement method (*i.e.*, INT [39]), and underwater image restoration methods (*i.e.*, RED [9], UWID [11] and UWIB [12]). In our experiments, the test images are captured under varying underwater scenes for generalization evaluation. For fair comparisons, we did not compare our method with WaterGAN since it was just available for underwater images captured under designated sites. We subjectively evaluate the visual quality of the results on our collected dataset including diversified underwater images. Then, we conduct a user study since there is no metric designed for underwater image color correction available. Finally, we carry out application test on visual tasks to give additional evidence.

A. Subjective assessment

We collected an underwater dataset including 500 underwater images with diversified content and tones. In Figure 4,

original CycleGAN produces blurring results because it tends to translate the content and structure of air image to the underwater image. GW method introduces color casts for some images when its assumption is not available. INT method just increases the brightness of underwater images because the prior learned from natural scenes is unavailable. Three underwater images restoration methods remove the haze effects and improve the contrast, however, the color is not well restored since the assumed underwater optical parameters do not hold in some underwater scenes. On the contrary, our method can totally remove the greenish and bluish tone from raw underwater images as if our results are taken in the air, which leads to better visual quality.

B. User study

To perform a visual comparison in an objective way, we randomly selected 30 underwater images from our collected dataset for user study. The results of different methods were randomly displayed on the screen and compared with the corresponding raw underwater images. After that, we invited 10 participants who had experience with image processing to score results. There is no time limitation for each participant. The scores range from 1 (worst) to 8 (best). As baseline, we set the scores of raw underwater images to 3. We expect that the good result has good contrast and visibility, abundant details, and the color like air image. On the contrary, the bad result has low contrast and visibility, blurring details, serious artifacts and noise, and inauthentic color. We first present the average visual quality scores of the results shown Figure 4 in Table I.

TABLE I
THE AVERAGE SCORES OF THE RESULTS PRESENTED IN FIGURE 4

Method	I1	I2	I3	I4	I5
Raws	3	3	3	3	3
CycleGAN	3.3	2.5	2.8	2.9	3.5
GW	1.4	1.7	3.8	3.5	3
INT	3.1	3.1	3.5	4.9	3
RED	6.4	3.8	5.3	3.5	4.5
UWID	3.1	4.5	5.9	5.4	5.9
UWBI	3.5	4.1	5.5	4.5	3.5
Ours	7.5	7.5	6.2	6.2	6.6

In Table I, our results received best scores, which indicated that, from a visual perspective, our method produces much better results. Additionally, the underwater image restoration

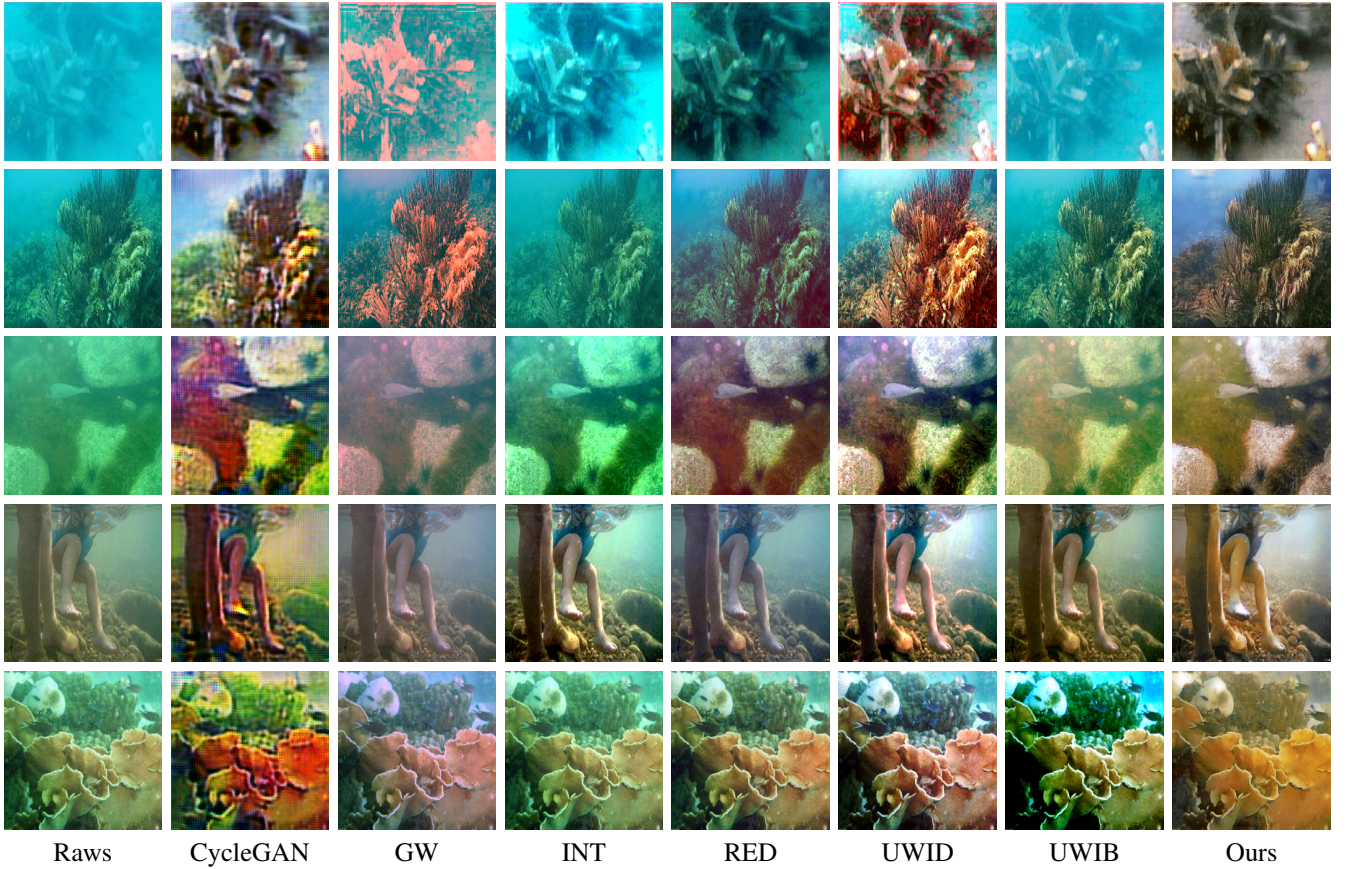


Fig. 4. Visual quality comparisons on varying underwater scenes. From top to bottom are image I1-I5.

methods also achieve good scores. The average visual quality scores for the selected 30 underwater images are 3, 2, 3, 3.3, 3.7, 4.6, 4, and 6.3 for Raws, CycleGAN, GW, INT, RED, UWID, UWBI, and Ours, respectively. Results and scores are made available in this [link](#). Those results provide a realistic feedback of our method generates visually pleasing results.

C. Application assessment

To further demonstrate the effectiveness of the proposed methods, we carry out several application tests including saliency detection [40] and keypoint matching [41]. In Figures 5 and 6, we present the results of application tests before and after using our method. For the limited space, we just present several examples. After color corrected by our method, the results achieve visually better saliency detection performance and more matching points. Application tests give additional evidence of the effectiveness of our method.

IV. CONCLUSION

In this letter, we presented a novel method for underwater image color correction. Based on the learned cross domain relations, the proposed method can remove color distortion by weakly supervised model. It is first attempt that correcting the color casts of underwater image by weakly supervised learning. Our method can be use as a guide for subsequent research of underwater image color correction. Experiments including quality assessment, user study, and application assessment, demonstrated the effectiveness of our method.

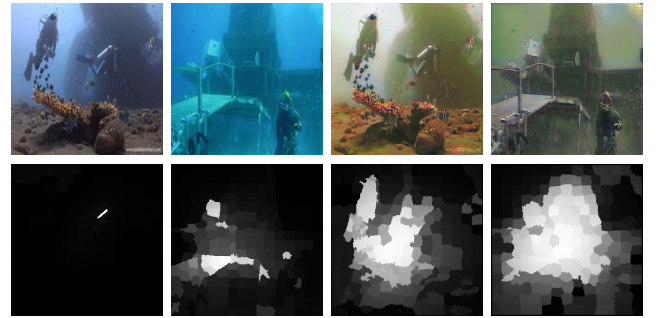


Fig. 5. Saliency test. From top to bottom are underwater images and the corresponding saliency detection results. From left to right are raw underwater images and our results.

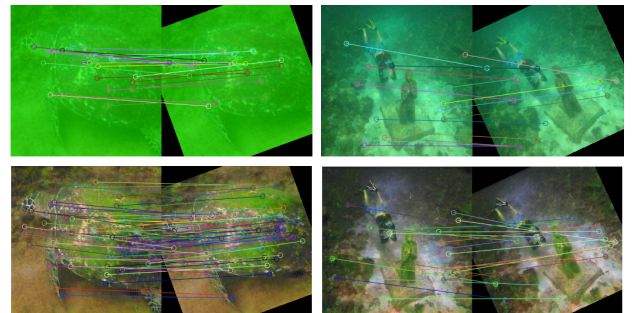


Fig. 6. Keypoint matching. From top to bottom are the keypoint matching results of raw underwater images and our results.

REFERENCES

- [1] M. Bryson, M. Johnson, O. Pizarro, and et al., "True color correction of autonomous underwater vehicle imagery," *J. Field Robot.*, vol. 33, no. 6, pp. 853-874, 2016.
- [2] R. Gibson, R. Atkinson, and J. Gordon, "A review of underwater stereo-image measurement for marine biology and ecology applications," *Oceanography and Marine Biology: An Annual Review*, vol. 47, pp. 257-292, 2016.
- [3] D. He and G. Seet, "Divergent-beam lidar imaging in turbid water," *Optics and Lasers in Eng.*, vol. 41, no. 1, pp. 217-231, 2004.
- [4] Y. Schechner and N. Karpel, "Clear underwater vision," in *Proc. IEEE Conf. Comput. Vis. Pattern Recognit.*, 2004, pp. xx.
- [5] Y. Schechner and N. Karpel, "Recovery of underwater visibility and structure by polarization analysis," *IEEE J. Oceanic Eng.*, vol. 30, no. 3, pp. 570-587, 2005.
- [6] T. Treibitz and Y. Schechner, "Active polarization descattering," *IEEE Trans. Pattern Anal. Mach. Intell.*, vol. 31, no. 3, pp. 385-399, 2009.
- [7] N. Carlevaris Bianco and A. Mohan and R. Eustice, "Initial results in underwater single image dehazing," in *Proc. of IEEE Conf. Oceans*, 2010, pp. 1-8.
- [8] J. Chiang and Y. Chen, "Underwater image enhancement by wavelength compensation and dehazing," *IEEE Trans. Image Process.*, vol. 21, no. 4, pp. 1756-1769, 2012.
- [9] A. Galdran, D. Pardo, and A. Picn, "Automatic red-channel underwater image restoration," *J. Vis. Commun. Image R.*, vol. 26, pp. 132-145, 2015.
- [10] P. Drews-Jr, E. Nascimento, S. Botelho, and et al., "Underwater depth estimation and image restoration based on single images," *IEEE Comput. Graph. Appl.*, vol. 36, no. 2, pp. 24-35, 2016.
- [11] C. Li, C. Ji, R. Cong, and et al., "Underwater image enhancement by dehazing with minimum information loss and histogram distribution prior," *IEEE Trans. Image Process.*, vol. 25, no. 12, pp. 5664-5677, 2016.
- [12] Y. Peng and P. Cosman, "Underwater image restoration based on image blurriness and light absorption," *IEEE Trans. Image Process.*, vol. 26, no. 4, pp. 1579-1594, 2017.
- [13] S. Emberton, L. Chittka, A. Cavallaro and et al., "Underwater image and video dehazing with pure haze region segmentation," *Computer Vision and Image Understanding*, 2017.
- [14] J. Li, K. Skinner, R. Eustice and et al., "WaterGAN: unsupervised generative network to enable real-time color correction of monocular underwater images," *IEEE Robot. and Aut. Lett.*, 2017.
- [15] S. Zhang, T. Wang, J. Dong and et al., "Underwater image enhancement via extended multi-scale retinex," *Neurocomputing*, vol. 245, pp. 1-9, 2017.
- [16] J. Ahn, S. Yasukawa, T. Sonoda and et al., "Enhancement of deep-sea floor images obtained by an underwater vehicle and its evaluation by crab recognition," *J. Marine Science and Technology*, vol. 22, no. 4, pp. 758-770, 2017.
- [17] R. Schettini and S. Corchs, "Underwater image processing: state of the art of restoration and image enhancement methods," *EURASIP J. Adv. Signal Process.*, 2010.
- [18] T. Haware and P. Gumble, "A review on underwater image scene enhancement and restoration using image processing," *Inter. J. Innovative. Research in Electrical, Electronics, Instrumentation and Control Engineering*, vol. 5, no. 9, pp. 28-31, 2017.
- [19] K. He, J. Sun, and X. Tang, "Single Image Haze Removal Using Dark Channel Prior," *IEEE Trans. Pattern Anal. Mach. Intell.*, vol. 33, no. 12, pp. 2341-2353, 2011.
- [20] Q. Zhu, J. Mai, and L. Shao, "A fast single image haze removal algorithm using color attenuation prior," *IEEE Trans. Image Process.*, vol. 24, no. 11, pp. 3522-3533, 2015.
- [21] K. Tang, J. Yang, and J. Wang, "Investigating haze-relevant features in a learning framework for image dehazing," in *Proc. of IEEE Conf. Comput. Vis. Pattern Recognit.*, 2014, pp. 2995-3002.
- [22] B. Cai, X. Xu, K. Jia, and et al., "DehazeNet: an end-to-end system for single image haze removal," *IEEE Trans. Image Process.*, vol. 25, no. 11, pp. 5187-5198, 2016.
- [23] G. Buchsbaum, "A spatial processor model for object colour perception," *J. of The Franklin Inst.*, vol. 310, no. 1, pp. 1-26, 1980.
- [24] E. Land, "The retinex theory of color vision," *Scientific American*, 1977.
- [25] M. Ebner, "Color Constancy," *Wiley 1st edition*, 2007.
- [26] G. Finlayson and E. Trezzi, "Shades of gray and colour constancy," in *Proc. of Color Imaging*, 2004, pp. 37-41.
- [27] I. Goodfellow, J. Pouget-Abadie, M. Mirza and et al., "Generative adversarial nets," in *Proc. of Adv. in Neur. Infor. Process. Sys.*, 2014, pp. 2672-268.
- [28] A. Radford, L. Metz, and S. Chintala, "Unsupervised representation learning with deep convolutional generative adversarial networks," in *Proc. of Int. Conf. Learn. R.*, 2016.
- [29] Y. Zhu, T. Park, P. Isola, and et al., "Unpaired image-to-image translation using cycle-consistent adversarial networks," *arXiv:1703.10593*, 2017.
- [30] T. Kim, M. Cha, H. Kim, and et al., "Learning to discover cross-domain relations with generative adversarial networks," *arXiv:1703.05192*, 2017.
- [31] M. Liu, T. Breuel, and J. Kautz, "Unsupervised image-to-image translation networks," *arXiv:1703.00848*, 2017.
- [32] Z. Wang, A. Bovik, H. Kautz, and et al., "Image quality assessment: from error visibility to structural similarity," *IEEE Trans. Image Process.*, 2004.
- [33] H. Zhao, O. Gallo, I. Frosio, and et al., "Loss functions for neural networks for image processing," *arXiv:1511.08861*, 2015.
- [34] J. Johnson, A. Alahi, and L. Fei-Fei, "Perceptual losses for real-time style transfer and super-resolution" in *Proc. of Eur. Conf. Comput. Vis.*, 2016, pp. 694-711.
- [35] P. Isola, J. Zhu, T. Zhou, and et al., "Image-to-image translation with conditional adversarial networks," *arXiv:1611.07004*, 2016.
- [36] C. Ledig, L. Theis, F. Huszar, and et al., "Photo-realistic single image superresolution using a generative adversarial network," *arXiv:1609.04802*, 2016.
- [37] C. Li and M. Wand, "Precomputed real-time texture synthesis with markovian generative adversarial networks" in *Proc. of Eur. Conf. Comput. Vis.*, 2016, pp. 702-716.
- [38] D. Kingma and J. Ba, "Adam: a method for stochastic optimization," *arXiv:1412.6980*, 2017.
- [39] Y. Gong and F. Sbalzarini, "A natural-scene gradient distribution prior and its application in light-microscopy image processing," *IEEE J. Sel. Topics Signal Process.*, vol. 10, no. 1, pp. 99-114, 2016.
- [40] H. Peng, B. Li, H. Ling, and et al., "Salient object detection via structured matrix decomposition," *IEEE Trans. Pattern Anal. Mach. Intell.*, vol. 39, no. 4, pp. 818-832, 2017.
- [41] H. Bay, T. Tuytelaars, and L. Van, "Surf: Speeded up robust features," in *Proc. of Eur. Conf. Comput. Vis.*, 2006, pp. 404-417.